International Journal of Computing and Digital Systems
ISSN (2210-142X)
Int. J. Com. Dig. Sys.13, No.1 (Mar-23)

http://dx.doi.org/10.12785/ijcds/130133

Performance Enhancement of Eulerian Video Magnification

Haider Ismael Shahadi[1], Zaid Jabbar Al-allaq[2], Hayder Jawad Albattat[2] and Hameed Rasool Farhan[1]

[1]*Electrical and electronic Engineering, University of Kerbala, 56001, Karbala, Iraq*
[2]*Communication Techniques Eng. Dept., Al-Furat Al-Awsat Technical University, 54003, Kufa, Iraq*

Received 21 Aug. 2021, Revised 13 Oct. 2022, Accepted 7 Mar. 2023, Published 16 Mar. 2023

Abstract: In this study, a linear and phase-based Eulerian video magnification (EVM) methods are developed to minimize magnified noises and processing time. The developed approaches utilize the Lanczos resampling algorithm to reduce the frames' size of the source video so that the size of the processed data is significantly reduced. Then spatial decomposition is applied to the resized frames. Subsequently, temporal filters with specific cut-off frequencies are also used to filter only the desired frequencies to be amplified and then add them to the decomposed frames. The magnified frames are processed by a wavelet denoising algorithm to locate distributed noise over the different frequency bands and then remove it. The resulted denoised-magnified frames are resized up and then reconstructed by the spatial synthesis process. The experiments show the superiority and effectiveness of the developed EVM approaches compared to the conventional ones and other related approaches in terms of the execution time and the quality of the magnified video. The developed EVM approach can be used in several applications such as the detection of human vital signs without contact so that it is very useful to avoid infection in several diseases such as Covid-19. Furthermore, it can be used in detection of human mood and lying detection, detection and localization of material and liquid variations.

Keywords: Eulerian video magnification (EVM), Linear-based EVM, Phase-based EVM, Lanczos resampling algorithm, wavelet denoising, computer vision applications, automatic motion detection.

1. Introduction

The real-life environment has small but meaningful temporal variations that ought to be detected and processed accordingly. However, these subtle variations are imperceptible for a human eye because of the limitation of the human vision system (HVS). Video media is a vessel of significant speed and subtle variations. Some of these variations contain useful information. For example, the arterial pulse in the human body is difficult to be seen, but the resulted movement from the pulse can be easily magnified based video magnification to measure pulse periods and heart rate [1], [2], [3], [4], [5].The slight chest motion can be amplified and utilized to measure the breathing activity. The method that is used for amplifying small variations in a video to be clear is called "Video magnification"[6].

Recently, several approaches have been proposed for video magnification. These approaches depend on computation and signal processing to visualize interest variations in the recorded videos. So, these approaches are operating as computer-based microscopes. The first approach had been proposed by Liu et al.[7]for hidden motion magnifying based on the Lagrange perspective. Because of the Lagrange based video magnification relies on pixel tracking and optical flow, the method is computationally intensive. Besides that, the magnified video frames has significant distortion that reflected directly to the magnified videos.

In 2012, a video magnification technique based on a linear Eulerian perspective was proposed and it was known as "Linear based Eulerian video magnification" (LB-EVM). The approach was produced by a research group at MIT by Hao et al.[8].It was based on the pixel's time series and amplification of variations in a certain temporal frequency band. The approach succeeded to amplify both colour changes and motions in videos, so it can exclude the expensive optical flow computations compare to [7].However, low magnification factors are supported because the magnification factor is proportional to the noise. Also, during the colour magnifying, an unwanted movement within the desired frequencies is also magnified. Therefore, in order to eliminate the linearity of Eulerian video magnification (EVM), Wadhwa et al.[9]have proposed a Phase based EVM (PB-EVM) approach. It is based on complex steerable pyramids that magnify phase-shift rather than the amplitude of the decomposed video frames [10], [11].The PB-EVM supports larger magnification factors with less noise than LB-EVM. However, it is so more complicated than LB-EVM.

Afterwards, several researches such as [12], [13], [14], [15], [16], [17] have attempted to develop and enhance

E-mail address: haider_almayaly@uokerbala.edu.iq, co j.zaid jabbar@atu.edu.iq, hayder.albattat@atu.edu.iq, hrf964@gmail.com

the EVM that is proposed by [8], [9].In [12], wavelet transform is used as a spatial decomposition to reduce the complexity of the algorithm. The method is fast compared to the EVM approaches. However, the magnification is also linearly proportional to the magnified noise. Moreover the unwanted motion can be magnified in case of the colour magnification. This is occurs because the low energy bands in the wavelet domains consist of subtle variations whether movement, colour, or noise. So, the magnified data is applied to all. Therefore, the noise and unwanted movement or colour variations are also magnified by the same ratio of the desired region. In [13], Le Liu et al. have enhanced LB-EVM to magnify the temporal motion of the video relying on an image warping. In comparison with LB-EVM technique, it supports higher amplification factors for low noise distortion. However, it requires a longer processing time than LB-EVM. In [17], authors have proposed a developed method based PB-EVM. The method uses Riesz pyramids to implement faster EVM. The main drawback of this method is that the quality of the magnified video is less than that in conventional PB-EVM.

In general, LB-EVM and PB-EVM are the two standards for video magnification and the other methods have attempted to develop these two standards. However, most methods focus to enhance one factor (processing time reduction, magnified noise reduction, magnification factor value (α)) without enhance or maintains the other important factors. Table I shows simple comparisons between the two EVM-standards and the other developed methods that mentioned above and they includes: enhanced EVM (E2VM) [13], Riesz pyramids for fast PB-EVM (RFPB-EVM) [17], and efficient motion magnification system (EMMS) [12].

From Table I, it is clearly that the mentioned methods still lacks one of the contrasting factors of the magnifications (processing time, magnification factor, magnified noise).

In our previous works [14], [15], [16] , time reduction for PB-EVM, and noise reduction for LB-EVM have been proposed. The developed approaches offered better results compare to the related methods. However, the combining of the two proposed approaches in a single approach gains the advantages of both together. Therefore, this paper proposes an improvement model for both PB-EVM and LB-EVM to effectively reduce the processing time and magnified noise together. The developed model uses Lanczos and wavelet denoising algorithms. The developed approach in this paper employ Lanczos resampling to resize-down the input video frames to significantly reduce the size of the processed data without effect the subtle information. Then after applying the magnification model, the magnified frames are processed by a wavelet denoising procedure to remove the magnified noise. Next, the resulted denoised-magnified frames are resized-up and reconstructed in its original input size. The proposed approach satisfy better results than the existing techniques in terms of magnified video quality and executing time. The developed EVM approach can be used in several applications such as the detection of the human vital signs without contact so that it is very useful to avoid infection in several diseases such as Covid-19. Also, it is enabled the doctors to avoid burned region that used in vital signs monitoring. Furthermore, it can be used in applications such as mood and lie detection, material and liquid variation detection.

The following sections are structured as follows: backgrounds of LB-EVM and PB-EVM are introduced in Section **??**. Section 3 describes the proposed technique using Lanczos interpolation and wavelet denoising algorithms. The developed EVM models are presented in Section **??**. The detailed explanation and discussion of the experimental results are introduced in Section 5. A comparison with the related approaches is done in Section 6. Finally, the main conclusions are presented in Section 7.

2. EULERIAN VIDEO MAGNIFICATION

As mentioned previously, EVM can be categorized as LB-EVM and PB-EVM. These two approaches are considered as the standards of the video magnifications. The steps of each category are briefly explained below.

A. LB-EVM

It is possible to achieve the small movement amplification by temporal processing using Taylor's first-order series extensions [18], [19]. LB-EVM processes the time series of the colour values of each pixel by amplifying a given range of interest frequencies in the temporal domain. First, input video frames are decomposed into separated frequency bands utilizing the entire Laplacian pyramid [20], [21], [22], [23]. The Laplacian pyramid is a data analysis structure in which the image size is down-sampled in successive periodic density until no further down-sampling is required.

Subsequently, decomposed bands by the Laplacian pyramid are filtered by temporal filters [8] to pass only the interest frequencies from each band. Thus, there is a need to amplify the interest regions of each band using a suitable magnification factor. Then, the original decomposed bands are added to the resulted magnified regions. Finally, the resulted added bands is subjected to the inverse Laplacian pyramid to get the magnified video frames. The structure of LB-EVM is illustrated in Fig. 1 This method is mathematically represented as in (2-A) for one-dimension signal, the equation is expanded to 2D and 3D as explained in detail in [8]:

$$\tilde{I}(x,t) = I(x,t) + \alpha B(x,t), \tilde{I}(x,t) \widehat{=} I(x,t) + \alpha B(x,t) \qquad (1)$$

$$B(x,t) = \delta(t)\frac{I(x,t)}{x} \qquad (2)$$

Where, I(x, t) represents the input image intensity at

TABLE I. COMPARISON BETWEEN SOME EVM APPROACHES.

Method	Pyramid method	Magnification factor (α)	Speed	Noise
LB-EVM [8]	Laplacian pyramid	Small, $\alpha < 25$	Fast speed	Magnified
E2VM [13]	Laplacian pyramid	Medium, $\alpha < 40$	15%–20% slower than LB-EVM	Minimized via post processing
PB-EVM [9]	Complex steerable pyramids	Large, α reach up to 150	300-400% slower tahn LB-EVM	Translated
RFPB-EVM [17]	Riesz pyramid	Large, α reach up to 100	About 30% faster than PB-EVM	Translated
EMMS [12]	Wavelet pyramid	Medium, $\alpha < 60$	About 50% faster than LB-EVM	Minimized

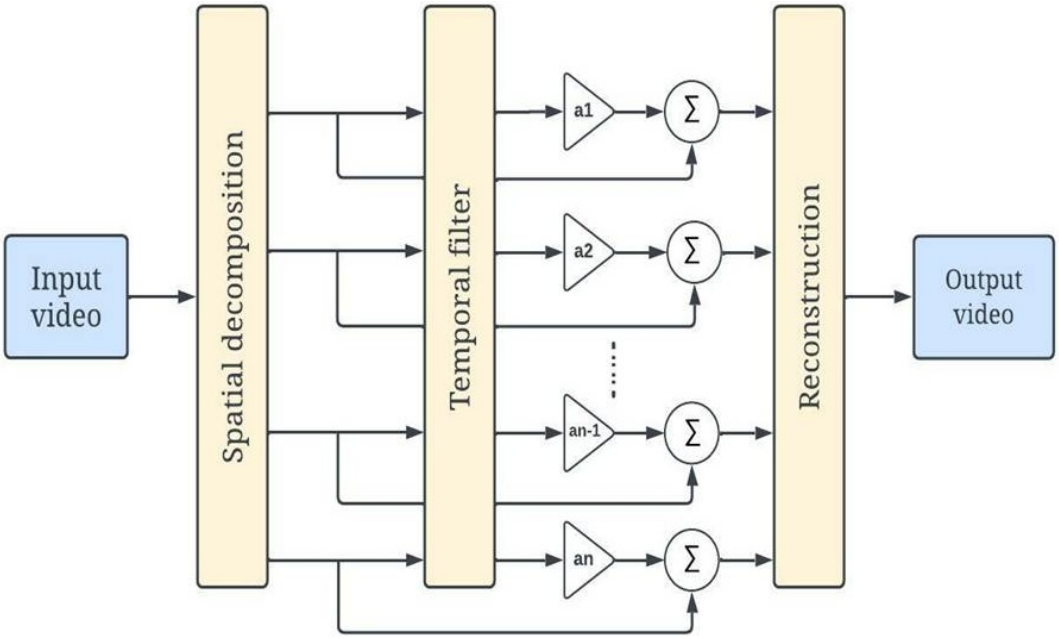

Figure 1. Illustration of LB-EVM scheme[8].

(x) position and (t) time; B(x, t) is the output of band-pass filtering the I(x, t); $\tilde{I}(x,t)$ is the magnified image; α is the magnification factor and $\delta(t)$ is the displacement function.The main disadvantage of LB-EVM is that the noise and unwanted changes (e.g. subtle movement) are magnified in the same linear proportion for the required regions of interest. As a result, distortion is increasing with the increase of the magnification factor [6]. Thus, this method is more useful at a small magnification factor.

B. PB-EVM

The phase-based optical flow is the basis of PB-EVM [24], [25], which improves LB-EVM since it has a best performance on noisy images and boosts higher magnification. However, it is more complicated in comparison with LB-EVM that magnifies temporal brightness changes so that the amplitude of noise is linearly magnified. PB-EVM does not magnify the amplitude so that spatial noise is not increased. Instead, the steerable pyramids detect the increases of differences in phase by a multiplier factor which could amplify unnoticed movements. Using Fourier analysis, images are analyzed into sub-domains and routed in the complex steerable pyramids, where the basis functions of the transformations are the same as Gabor waves [26]. The long processing time is the main disadvantage of this method [6]. The PB-EVM block diagram is illustrated in Fig.2.

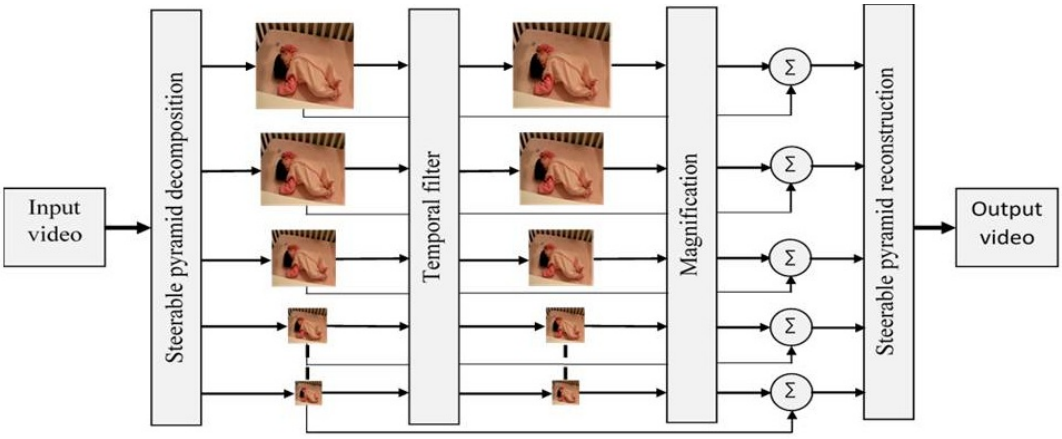

Figure 2. General structure of PB- EVM approach.

3. THE PROPOSED TECHNIQUE

The two critical problems in the conventional models of LB-EVM and PB-EVM are high distortion in the magnified videos and long processing time, respectively. In order to overcome these problems, we propose adding the following pre-processing and post-processing schemes to the conventional EVM models:

1.Lanczos-3 interpolation technique.

2.Wavelet denoising technique.

The Lanczos interpolation technique will reduce the computation and eventually processing required by the algorithm. The wavelet denoising scheme will reduce the distortion presented in the magnified video.

A. *Lanczos-3 Interpolation*

Cornelius Lanczos have proposed an interpolation algorithm that is very useful in image resizing processes, which is called Lanczos version-3 interpolation [27], [28]. The Lanczos-3 interpolation provides a smoother interpolation compared to bi-cubic algorithm. It is a type of a Fourier kernel filter, which consists of the multiplication of two SINC functions [29]. The main formula for a resizing filter is implementing by a SINC function, as shown in (3) for one-dimension input.

$$L(x) = \begin{cases} 1 & x = 0 \\ \frac{a\sin(\pi x)\sin(\frac{\pi x}{a})}{\pi^2 x^2} & 0 < |x| < a \\ 0 & otherwise \end{cases} \tag{3}$$

Where, a represents the filter size, which is a positive integer number.

Let S_i be the samples of a one-dimension vector, where i represents the sample's number. The kernel filter at a random real argument x is obtained by the interpolated value $S(x)$ as follows:

$$S(x) = \sum_{i=\lfloor x \rfloor - a+1}^{\lfloor x \rfloor + a} S_i L(x - i) \tag{4}$$

A two-dimension array is manipulated as two one-dimension array, where the Lanczos kernel can be calculated as in (5) from the product of the two arrays of Kernel filters.

$$L(x, y) = L(x)L(y) \tag{5}$$

The interpolated or reconstructed matrix of a two-dimension array e.g. S_{ij} is obtained as in (6), where i and j are the indices of the row and column, respectively.

$$S(x, y) = \sum_{i=\lfloor x \rfloor - a+1}^{\lfloor x \rfloor + a} \sum_{j=\lfloor y \rfloor - a+1}^{\lfloor y \rfloor + a} S_{ij} L(x - i)L(y - j) \tag{6}$$

In case of down resized images, the reconstructed matrix is highly identical to the original matrix view as well as the smoothness.

B. *Wavelet denoising technique*

In this work, a wavelet-based denoising approach has been used to reduce magnified noise. The stages of the approaches are shown in Fig. 3 and listed as follows:

i) Wavelet transform (WT), ii) Threshold estimation and application, and iii) Inverse wavelet transform (IWT).

WT is a great signal processing tool that can be utilized in two-dimension signals such as images. The transform localizes frequency contents of the image. In wavelet approach, images are decomposed into different frequency levels. Through the use of low and high pass filters, the transform divides the original image into four bands for each level of decomposition: LL, HL, LH, and HH. LL sub-band represents the approximate version of the original image. The remaining three sub-bands represent the details

Figure 3. Image denoising approach based Wavelet algorithm.

of wavelet coefficients. Fig. 4(a) shows one-level of decomposition that produces the sub-bands HL1, HH1 and LH1 as the detail coefficients, whereas the sub-band LL1 denotes the coefficients of the low level [30], [31]. The 2nd level of decomposition is achieved through further decomposing LL1 sub-band, as illustrated in Fig. 4(b).

After decomposition, the wavelet threshold is selected to analyze the specific wavelet coefficients. Wavelet threshold is a signal estimation technique that makes use of the WT multi-resolution decomposition in both time and frequency domain, therefore; it easily localizes the noise in the image. The fundamental threshold kinds are soft and hard thresholds. The wavelet coefficients are reset to zero in a hard threshold when they are lower than the threshold; else, they remain as it is unchanged [32].

This method is produced a large number of artificial noise points at the images edges, which leads to image deformation. The resulting wavelet coefficients values (y) are decided by (7) which sets the original value coefficient (x) if the value is above (Thr), and otherwise it is set to zero.

$$y = \begin{cases} x & if\ |x| > Thr \\ 0 & if\ |x| < Thr \end{cases} \tag{7}$$

In the soft threshold, the threshold values are chosen according to the image visual interest [33]. It has the ability to overcome the flaws of the hard threshold algorithm. Consequently, the resulted coefficients are comparatively smooth. The function for a soft threshold is given by (8).

$$y = \begin{cases} sgn(x) \times (|x| - Thr) & if\ |x| > Thr \\ 0 & otherwise \end{cases} \tag{8}$$

Where, y is the signal after taking the threshold value into account, x is the original wavelet coefficient, and Thr is the threshold level.

In this work, the soft threshold technique has been chosen to be applied after five levels of DWT decomposition. Daubechies type 4 (db4) has been chosen as a mother function in WT. The final step in the denoising algorithm is applying IWT to attain the reconstructed image with better noise performances [34].

4. THE DEVELOPED EVM MODEL USING THE PROPOSED TECHNIQUE

This section illustrates the developed EVM approach based on the proposed schemes. The modified EVM maintains the advantages of (LB-EVM and PB-EVM), and also overcomes their disadvantages. This is achieved by adding the two pre-processing and post-processing schemes to the conventional EVM-models (LB-EVM and PB-EVM).

The developed model stars by resampling-down the input video frames using Lanczos-3 interpolation. Then, conventional EVM is applied and the magnified video frames are resampled-up. This procedure significantly reduces the processing time. In denoising scheme based-WT; the magnified video frames are decomposed in a way to locate exactly the wanted subtle variations(motion or colour) to be amplified and attenuate unwanted subtle variations (colour, motion, or noise). This stage will reduce the noise (distortion) generated in the magnified video frames. Fig. 5 illustrates the block diagram of the developed EVM.

The developed EVM approaches (linear and phased-based) compromise between noise performance and processing time to verify a fast EVM that is suitable for large magnification factors because of its good noise performances.

The steps of the developed EVM models are explained below. In order to display the output, the baby video is considered as input to the algorithm.

1) Step 1: Reading the input video file that is formatted as .avi. Fig. 6(a) shows the first frame of the input video.
2) Step 2: Applying Lanczos-3 resampling method. In this stage, the frames' sizes of the input video are reduced by 50% to produce frames of size 25% of the original frame's size. Fig. 6(b) shows the resulted first frame for the taken example after accomplishing this step.
3) Step 3: Transforming the obtained frames from RGB to YIQ colour format. The illumination information are indicated by the Y component, whereas the chrominance information are represented by the I and Q components. The YIQ model has an advantage over RGB model due to the characteristics of human response to the colours. As the human eye is more sensitive to the intensity of light than to colour, and also when using another colour space in magnify (for example RGB), we get a lower information about the subtle information in the image. Eq. (9) is used to

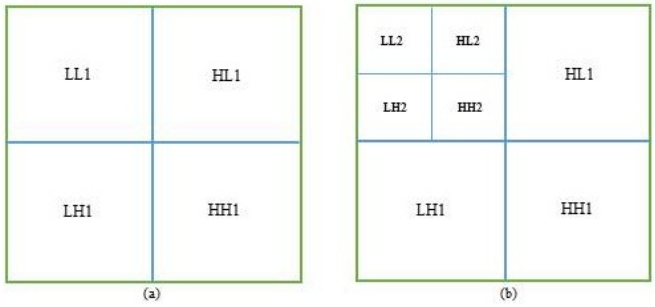

Figure 4. (a) One-level decomposition (b) Two-level decomposition.

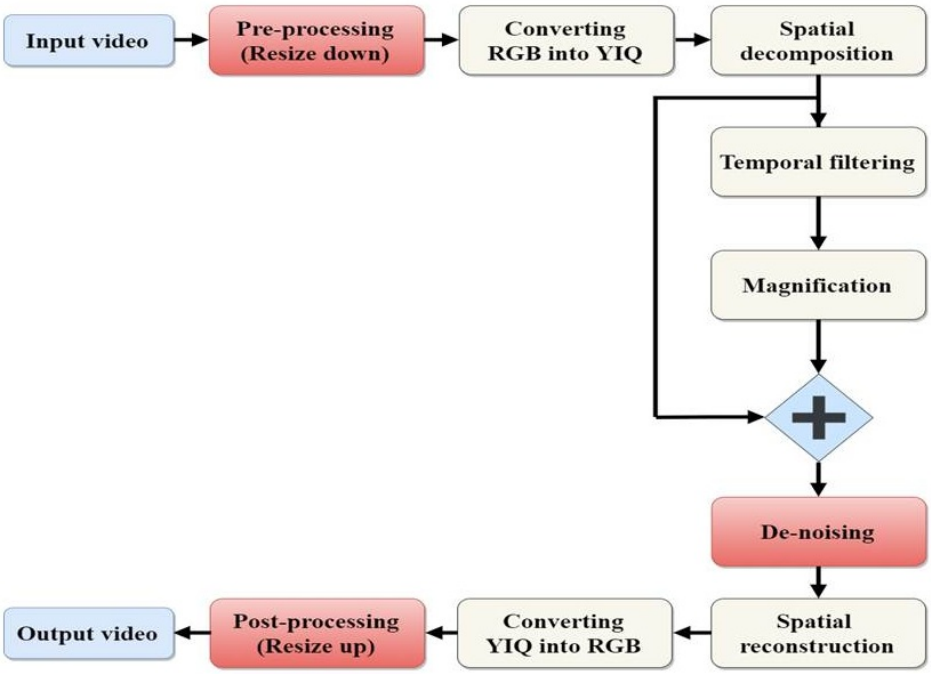

Figure 5. The processing stages of the developed EVM model.

confirm such transformation on the resized frames. Fig. 6(c) demonstrates the produced Y-channel of the resized first frame.

$$\begin{bmatrix} Y \\ I \\ Q \end{bmatrix} = \begin{bmatrix} 0.299 & 0.587 & 0.114 \\ 0.596 & -0.274 & -0.322 \\ 0.211 & -0.523 & 0.312 \end{bmatrix} \begin{bmatrix} R \\ G \\ B \end{bmatrix} \quad (9)$$

4) Step 4: Applying the Laplacian pyramid decomposition, in the case of using LB-EVM, on the Y-channel of each video frame to decompose the input video frames into various spatial bands. Fig.7(a) shows the Laplacian pyramid for our example at 4-level decomposition. Whilst in PB-EVM, applying the steerable pyramid decomposition [9] on each plane of the video frames (Y, I, and Q). The output of the steerable pyramid decomposition for our example based on Y-layer only is shown in Fig.7(b) at phase 0 and 900, and two scales from the pyramid are taken.
5) Step 5: Temporal filtering is applied to the resulted bands from the previous steps to allow the concern bands of frequencies for passing into the amplifying stage. Low-order of IIR and FIR filters are used according to the input video. Subsequently, the filtered frames are magnified through the use of a suitable magnification factor that is multiplied by the resulted frequency band from the temporary filter.
6) Step 6: After combining the resulted bands from the pyramid decomposition with the amplified bands, a reconstruction process of Laplacian or Steerable pyramid is accomplished according to the type of the magnification method; LB-EVM or PB-EVM, respectively. Fig.8(a) shows the first magnified frame of our example.

Figure 6. Examples of the resulted frame from the resizing and YIQ-conversion steps.

7) Step 7: The wavelet denoising algorithm is applied to eliminate the magnified noise from the magnified frames. The db4 wavelet function is used with five levels of WT, and the denoising process is subjected to a soft threshold. The resulted wavelet coefficients are reconstructed by five levels of wavelet synthesis. The output of the denoising step is shown in Fig.8(b). The difference in quality before and after applying the wavelet denoising algorithm can clearly be seen.
8) Step 8: Transforming the magnified frames from YIQ model to RGB model to retrieve the original video colour. Eq. (10) is applied on each frame to achieve this transformation. Fig.8(c) displays the result of this step for the first frame of our example.

$$\begin{bmatrix} R \\ G \\ B \end{bmatrix} = \begin{bmatrix} 1 & 0.956 & 0.619 \\ 1 & -0.272 & -0.647 \\ 1 & -1.106 & 1.703 \end{bmatrix} \begin{bmatrix} Y \\ I \\ Q \end{bmatrix} \quad (10)$$

9) Step 9: Finally, up resizing the resulted frames by 200 % of the height and width of the resulted video frames to return the magnified video to its original size. In this step, we also use the same Lanczos-3 resampling method. Fig.8(d) shows the final result for the first frame from our example.

5. EXPERIMENTS AND DISCUSSION

To evaluate the performance of the developed EVM, objective quality metrics are utilized. These metrics are modified to be applied to the video dimension:

A. Peak signal-to-noise ratio (PSNR)

PSNR is calculated for the resulted video frames according to (11) to evaluate the video quality, where the square of the largest pixel intensity value (255) is divided by the mean square error (MSE) of each video frame. After that, the final required PSNR is calculated by averaging the PSNR values of all video frames.

$$PSNR = 10\log(\frac{255^2}{MES})$$

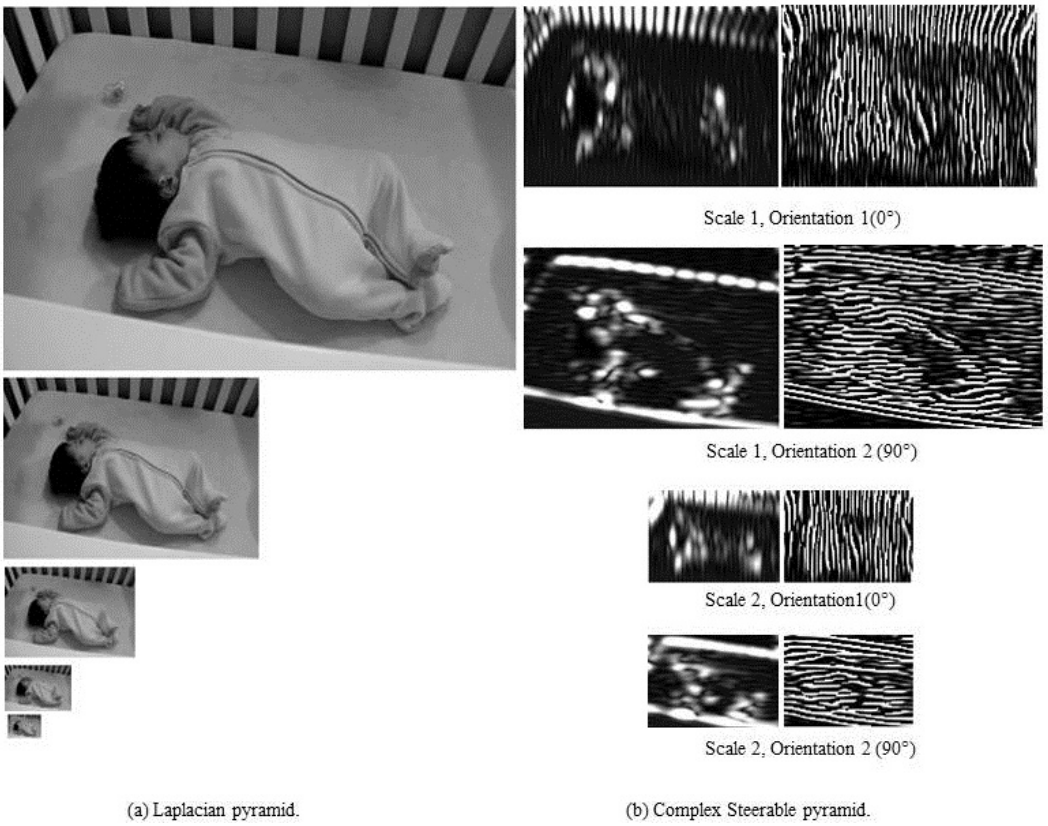

Figure 7. Examples of the pyramid decomposition results.

$$MSE = \frac{1}{N \times M} \sum_{k=1}^{3} \sum_{i=1}^{N} \sum_{j=1}^{M} \left[\left[(I_{i,j} - Ia_{i,j}) \right]^2 \right] \quad (11)$$

Where, I is the original frame, Ia is the amplified frame, N and M are the frame dimensions, and k is the layer number in each frame (R,G,and B).

B. Maximum Error (MAXER)

is the absolute maximum squared deviation between input and output video frames as shown in (12).

$$MAXER = \frac{\sum_{i=1}^{N} \sum_{j=1}^{M} (I_{i,j} - \widehat{I}_{i,j})}{N * M} \quad (12)$$

Where: I and I are the original and the amplified frames respectively, M and N are the frame dimensions .

C. Energy ratio of the square norm (L2RAT)

ratio of the normalized output to the normalized input video frames as shown in (13).

$$L2RAT = \frac{norm\left[\widehat{I}\right]^2}{norm\,[I]^2} \quad (13)$$

Where: I is the input frame, I is the magnified frame.

D. Blind reference-less Image Spatial Quality Evaluator (BRISQUE)

The BRISQUE algorithm allows for determining the perceived quality by employing a model depend on natural images with self-ratings instead of a reference image as shown in (14). After training the model, it indicates the apparent quality better than PSNR [35]. The score range [0; 100] represents values of BRISQUE, where the numbers close to 0 refers to better quality.

$$\widehat{I}(i,j,k) = \frac{I(i,j,k) - \mu(i,j,k)}{\sigma(i,j,k) + c} \quad (14)$$

Where, $I(i,j,k)$ represents the intensity of the input frame, (i,j,k) is the local mean, (i,j,k) is the local variance, and c is a small constant approximately equal to 1; it is used to prevent the denominator from being equals to zero, which causes an instability.

All the experimental results are achieved using Matlab version 2017-b.The videos used in the tests are shown in Fig.9 that have AVI format and sizes as follows:Baby1 source video has 301 frames, where the frame rate is 30 frames per second (FPS) and the frame size is 960×544 ×3. Baby2 source video has a frame size of 640×352 ×3, 900 frames, and a frame rate of 30 FPS. Baby3 source

(a) Magnified frame. (b) Frame after denoising.

(c) Reconstructed RGB frame.

(d) Frame after resizing-up.

Figure 8. Sample results to show the steps of obtaining magnified frame.

video has a frame size of 1280×720×3, 222 frames, and 30 FPS frame rate. Eye source video has a frame rate of 30 FPS, frame size of 1152×896×3, and 140 frames. Face source video has a frame a rate of 30 FPS, frame size of 528×592×3, and 301 frames. Camera source video has a frame size of 512×384×3, 1001 frames, and a frame rate of 300 FPS. All the videos except Baby3 have been downloaded from the MIT website, whereas the Baby3-video has been recorded for a baby is casualty viral hepatitis in central child hospital - Iraq. The presented results are compared to conventional EVM and also to relevant work. Five methods have been used in our comparison that includes: conventional LB-EVM [8], conventional PB-EVM [9], enhanced EVM (E2VM) [13], Riesz pyramids for fast PB-EVM (RFPB-EVM) [17], and efficient motion magnification systems (EMMS) [12].

5.1 *Comparison between the developed and conventional LB-EVM*

Three videos (Baby1, Baby2, and Face) have been used in the comparison tests as illustrated in Table II. Both the processing time and noise are extremely reduced, where the processing time is reduced to about 50% and the magnified video quality is highly enhanced. Table II also shows the comparison tests at large magnification factors. Figs. 10 and

Figure 9. Source videos used in the experiments.

11 show samples of the source frames and magnified frames by conventional and developed LB-EVM at magnification factor α=30 and α=200, respectively. It clearly seems from (Figs. 10 and 11) the superiority of the developed method over the conventional LB-EVM. In order to show the results visually through a video file, some video results related to the comparison of the developed and conventional LB-EVM have been uploaded on YouTube (Please refer to the link in https://youtu.be/pk$_U$6Xz1GVo.).

5.2 *Comparison between the developed and conventional PB-EVM*

Results in Table III presents the comparison tests between developed and conventional PB-EVM. Three source videos have been used in the tests include: Baby1, Baby3, and Eye. Large magnification factors are used in the tests (100 and 200). Both the processing time and noise in the magnified videos are extremely reduced. Where the processing time is reduced to about 60% and the magnified video qualities are highly enhanced. Fig. **??** shows a sample from the source frames, and the magnified frames using the conventional and developed PB-EVM at α =200. It is clear that the quality of the developed PB-EVM frames are much better than that of the conventional one. Moreover, the processing time is reduced to about 60% of that of the conventional method. The difference in quality and processing time are also illustrated very clear in the video file that is uploaded on YouTube to compare between the conventional and developed PB-EVM (Please refer to the link in https://youtu.be/pk$_U$6Xz1GVo).

6. COMPARISON BETWEEN THE DEVELOPED EVM AND OTHER TECHNIQUES

The performance of the developed EVM models are also compared to related work as explained below:

1) Comparison between the developed LB-EVM and E2VM method [13]:

Table IV shows a comparison between E2VM and the developed LB-EVM using Baby1 as a source video at α=20. The developed LB-EVM achieves a time reduction of about 50% compared to the conventional one, while E2VM consumes a processing time of 14.5% above the conventional LB-EVM [13]. Moreover, E2VM still has significant distortion at large magnification factors.

2) Comparison between the developed PB-EVM and the RFPB-EVM method [17]:

Table V shows a comparison between RFPB-EVM and the developed PB-EVM using Baby1 and Camera as source videos. The RFPB-EVM is faster than the conventional PB-EVM. However, the quality of the magnified video is less than that of PB-EVM. Therefore, this method fails when using the large magnification factors. In contrast, the developed PB-EVM reduces the time by 60% and produces better video quality.

Figure 10. Samples of Baby1 video before and after magnification using conventional and developed LB-EVM approaches at α=30.

3) Comparison between the developed PB-EVM and the EMMS method [12]:

Table VI shows a comparison between EMMS and the developed PB-EVM using Baby1 and Camera as source videos. EMMS reduces the implementation time but it remains within the limits of using the small magnification factor. Because the noise is linearly magnified as colour and motion. The reason for linear magnification here is due to the concept that the WT divides the image between both frequency and spatial domain into different bands. The noise and subtle changes required to be magnified are both located in the same bands especially in high-frequency bands. Therefore, the noise and unwanted motion or colours are magnified also by the same ratio of wanted changes. As a result, the distortion appears in the magnified frames at large magnification factors. In contrast, the developed PB-EVM is able to reduce the implementation time significantly and improve the quality of the resulting video by reducing the noise.

7. CONCLUSIONS

This paper has developed an efficient EVM based on the standard (LB-EVM and PB-EVM). The developed approaches reduce the processing time by more than 50% and at the same time enhance the noise performance of the magnified videos. The developed technique can easily magnify invisible motion or colour variations in the video frame to be detectable to the naked eye. Wavelet transform is employed to remove the magnified distortion from video frames by localize the frequency bands that consists the noise, and the Lanczos-3 kernel filter is utilized to reduce the size of the processed data by EVM without effect the subtle information. The experimental results of the developed approach have shown that it is superior in both processing time and noise performance compared to the standard EVM models and other related approaches. This allows the developed EVM to magnify subtle motion and colour change by larger magnification factor compare to the other approaches. Therefore, the developed EVM can be used in different applications. For example, it can be used to measure the accurate human vital signs such as

(a) Source frames (frame number 10, 33, and 42).

(b) Amplified frames using conventional LB-EVM.

(c) Amplified frames using the developed LB-EVM.

Figure 11. Samples of Face video before and after magnification using conventional and developed LB-EVM approaches at α=200.

heart rate, oxygen percentage in blood, body temperature, and breathing monitoring for patients that have infected diseases such as COVID-19, burned region of body, and low immunity. Furthermore, it can be employed in scientific applications such as chemistry to monitor the variations during interactive, physics to monitor metal changes versus temperature and other parameters. For future work, complex wavelet can be employed instead steerable pyramids to magnify the phase of motion instead pixel's intensity.

References

[1] A. Al-Naji and J. Chahl, "Noncontact heart activity measurement system based on video imaging analysis," *International Journal of Pattern Recognition and Artificial Intelligence*, vol. 31, no. 02, p. 1757001, 2017.

[2] X. He, R. A. Goubran, and X. P. Liu, "Wrist pulse measurement and analysis using eulerian video magnification," in *2016 IEEE-EMBS International Conference on Biomedical and Health Informatics (BHI)*. IEEE, 2016, pp. 41–44.

[3] M.-Z. Poh, D. J. McDuff, and R. W. Picard, "Advancements in noncontact, multiparameter physiological measurements using a

TABLE III. COMPARISON BETWEEN CONVENTIONAL AND DEVELOPED PB-EVM.

Input video		Baby1		Eye		Baby3	
Frequencies of BPF (Hz)		0.1 - 0.4		30 - 50		0.2 - 0.4	
σ		5		4		5	
α		100	200	75	85	100	150
Conventional PB-EVM [9]	Processing Time (s)	231.73	231.33	211.94	211.88	247.89	248.54
	PSNR (db)	27.25	25.08	32.53	32.25	32.01	31
	MSE	122.48	201.87	36.31	38.73	40.93	51.65
	MAXER	145.17	155.99	206.73	209.30	162.16	169.21
	L2RAT	0.9962	0.9891	0.9925	0.9917	0.9970	0.9949
Developed PB-EVM	Processing Time (s)	90.69	90.28	108.97	108.69	76.59	76.86
	PSNR (db)	36.09	33.53	35.63	35.37	37.20	36.13
	MSE	15.99	28.85	17.79	18.88	12.39	15.85
	MAXER	123.96	138.62	139.64	141.99	116.40	128.20
	L2RAT	0.9990	0.9986	0.9900	0.9897	0.9994	0.9989

webcam," *IEEE transactions on biomedical engineering*, vol. 58, no. 1, pp. 7–11, 2010.

[4] M.-Z. Poh, D. J. McDuff, and R. W. Picard, "Non-contact, automated cardiac pulse measurements using video imaging and blind source separation." *Optics express*, vol. 18, no. 10, pp. 10 762–10 774, 2010.

[5] W. Verkruysse, L. O. Svaasand, and J. S. Nelson, "Remote plethysmographic imaging using ambient light." *Optics express*, vol. 16, no. 26, pp. 21 434–21 445, 2008.

[6] H. I. Shahadi, H. J. Albattat, Z. J. Al-allaq, and A. T. Thahab, "Eulerian video magnification: A review," *Indones. J. Electr. Eng. Comput. Sci*, vol. 18, pp. 799–811, 2020.

[7] C. Liu, A. Torralba, W. T. Freeman, F. Durand, and E. H. Adelson, "Motion magnification," *ACM transactions on graphics (TOG)*, vol. 24, no. 3, pp. 519–526, 2005.

[8] H.-Y. Wu, M. Rubinstein, E. Shih, J. Guttag, F. Durand, and W. Freeman, "Eulerian video magnification for revealing subtle changes in the world," *ACM transactions on graphics (TOG)*, vol. 31, no. 4, pp. 1–8, 2012.

[9] N. Wadhwa, M. Rubinstein, F. Durand, and W. T. Freeman, "Phase-based video motion processing," *ACM Transactions on Graphics (TOG)*, vol. 32, no. 4, pp. 1–10, 2013.

[10] E. P. Simoncelli, W. T. Freeman, E. H. Adelson, and D. J. Heeger, "Shiftable multiscale transforms," *IEEE transactions on Information Theory*, vol. 38, no. 2, pp. 587–607, 1992.

[11] J. Portilla and E. P. Simoncelli, "A parametric texture model based on joint statistics of complex wavelet coefficients," *International journal of computer vision*, vol. 40, no. 1, pp. 49–70, 2000.

[12] A. Al-Naji, S.-H. Lee, and J. Chahl, "An efficient motion magnification system for real-time applications," *Machine Vision and Applications*, vol. 29, no. 4, pp. 585–600, 2018.

[13] L. Liu, L. Lu, J. Luo, J. Zhang, and X. Chen, "Enhanced eulerian video magnification," in *2014 7th International Congress on Image and Signal Processing*. IEEE, 2014, pp. 50–54.

[14] H. I. Shahadi, Z. J. Al-Allaq, and H. J. Albattat, "Efficient denoising approach based eulerian video magnification for colour and motion variations." *International Journal of Electrical & Computer Engineering (2088-8708)*, vol. 10, no. 5, 2020.

[15] H. I. Shahadi, Z. J. Al-allaq, and H. J. Albattat, "Developed approach for phase-based eulerian video magnification," *Telkomnika*, vol. 18, no. 5, pp. 2391–2400, 2020.

[16] Z. J. Al-allaq, H. I. Shahadi, and H. J. Albattat, "Powerful and low time phase-based video magnification enhancing technique," in *2019 4th Scientific International Conference Najaf (SICN)*. IEEE, 2019, pp. 133–138.

[17] N. Wadhwa, M. Rubinstein, F. Durand, and W. T. Freeman, "Riesz pyramids for fast phase-based video magnification," in *2014 IEEE International Conference on Computational Photography (ICCP)*. IEEE, 2014, pp. 1–10.

[18] B. K. Horn and B. G. Schunck, "Determining optical flow," *Artificial intelligence*, vol. 17, no. 1-3, pp. 185–203, 1981.

[19] B. D. Lucas, T. Kanade *et al.*, "An iterative image registration technique with an application to stereo vision." Vancouver, 1981.

[20] E. H. Adelson, C. H. Anderson, J. R. Bergen, P. J. Burt, and J. M. Ogden, "Pyramid methods in image processing," *RCA engineer*, vol. 29, no. 6, pp. 33–41, 1984.

[21] J.-Y. Bouguet *et al.*, "Pyramidal implementation of the affine lucas kanade feature tracker description of the algorithm," *Intel corporation*, vol. 5, no. 1-10, p. 4, 2001.

[22] P. J. Burt, "Eh adelson the laplacian pyramid as a compact image code," *IEEE Transactions on Communications*, vol. 31, no. 4, pp. 532–540, 1983.

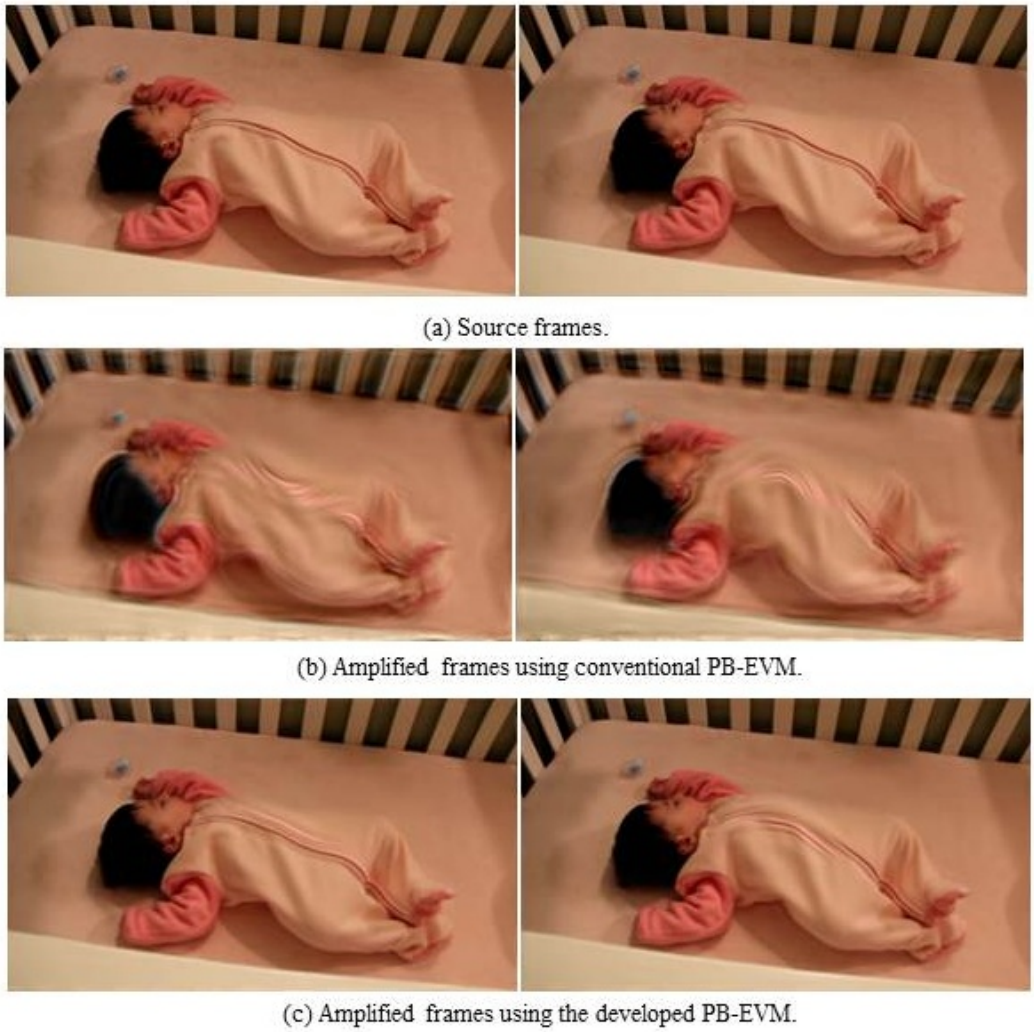

(a) Source frames.

(b) Amplified frames using conventional PB-EVM.

(c) Amplified frames using the developed PB-EVM.

Figure 12. Samples of Baby1 video before and after magnification at α =200 using the conventional and developed PB-EVM.

TABLE IV. COMPARISON BETWEEN E2VM AND THE DEVELOPED LB-EVM USING BABY1 AS SOURCE VIDEO AT α =20.

Method	PSNR (db)	Processing Time
E2VM [13]	34.91	Increased by 14.5 %
Developed LB-EVM	38.89	Decreased by 50 %

TABLE V. Comparison between RFPB-EVM and the developed PB-EVM.

Input video		Baby1	Camera
Frequencies of BPF (Hz)		0.1 - 0.4	36 - 62
α		10	60
RFPB-EVM [17]	PSNR (db)	34.08	32.32
	MSE	25.41	38.08
Developed PB-EVM	PSNR (db)	43.95	39.72
	MSE	2.62	6.94

TABLE VI. COMPARISON BETWEEN EMMS AND THE DEVELOPED PB-EVM.

Input video		Baby1	Camera
α		20	100
EMMS [12]	PSNR (db)	39.44	36.95
	MSE	7.48	13.11
Developed PB-EVM	PSNR (db)	40.06	37.26
	MSE	6.41	12.22

[23] W. T. Freeman, E. H. Adelson, and D. J. Heeger, "Motion without movement," *ACM Siggraph Computer Graphics*, vol. 25, no. 4, pp. 27–30, 1991.

[24] D. J. Fleet and A. D. Jepson, "Computation of component image velocity from local phase information," *International journal of computer vision*, vol. 5, no. 1, pp. 77–104, 1990.

[25] T. Gautama and M. Van Hulle, "A phase-based approach to the estimation of the optical flow field using spatial filtering," *IEEE transactions on neural networks*, vol. 13, no. 5, pp. 1127–1136, 2002.

[26] W. Jiang, T.-Z. Shen, J. Zhang, Y. Hu, and X.-Y. Wang, "Gabor wavelets for image processing," in *2008 ISECS International Colloquium on Computing, Communication, Control, and Management*, vol. 1. IEEE, 2008, pp. 110–114.

[27] T. Moraes, P. Amorim, J. Silva, and H. Pedrini, "3d lanczos interpolation for medical volumes," in *15th International Symposium on Computer Methods in Biomechanics and Biomedical Engineering*, 2018, pp. 1–10.

[28] D. S. Yoo, J. Chang, C. H. Park, and M. G. Kang, "Video resampling algorithm for simultaneous deinterlacing and image upscaling with reduced jagged edge artifacts," *EURASIP Journal on Advances in Signal Processing*, vol. 2013, no. 1, pp. 1–24, 2013.

[29] P. S. Parsania and P. V. Virparia, "A comparative analysis of image interpolation algorithms," *International Journal of Advanced Research in Computer and Communication Engineering*, vol. 5, no. 1, pp. 29–34, 2016.

[30] P. Patidar, M. Gupta, S. Srivastava, and A. K. Nagawat, "Image denoising by various filters for different noise," *International journal of computer applications*, vol. 9, no. 4, pp. 45–50, 2010.

[31] H. I. Shahadi, R. Jidin, and W. H. Way, "High performance fpga architecture for dual mode processor of integer haar lifting-based wavelet transform," *Int. Rev. Comput. Softw*, vol. 8, no. 9, pp. 2058–2067, 2013.

[32] Y. Liu, "Image denoising method based on threshold, wavelet transform and genetic algorithm," *International Journal of Signal Processing, Image Processing and Pattern Recognition*, vol. 8, no. 2, pp. 29–40, 2015.

[33] M. Saha, M. K. Naskar, and B. Chatterji, "Soft, hard and block thresholding techniques for denoising of mammogram images," *IETE Journal of Research*, vol. 61, no. 2, pp. 186–191, 2015.

[34] D. Kumar and V. Kukreja, "N-cnn based transfer learning method for classification of powdery mildew wheat disease," in *2021 International Conference on Emerging Smart Computing and Informatics (ESCI)*. IEEE, 2021, pp. 707–710.

[35] A. Mittal, A. K. Moorthy, and A. C. Bovik, "No-reference image quality assessment in the spatial domain," *IEEE Transactions on image processing*, vol. 21, no. 12, pp. 4695–4708, 2012.

Haider Ismael Shahadi received his B.ESc degree in information engineering from the University of Baghdad, Iraq in 2001, his master's degree in Electronic and Communication Engineering from the University of Baghdad-Iraq in 2004, and his Ph.D. in Electronic and Communication Engineering from the Tenaga National University, Malaysia in 2014. Currently, he is an assistant professor at the University of Kerbala, Iraq. His research interests include digital signal and multimedia processing, data security, FPGA design and implementation and embedded systems, IOT systems, and smart systems.and a short biography.

Zaid Jabbar Al-allaq received a B.ESc degree in Communication Techniques Engineering from the Engineering Technical College, Al-Furat Al-Awsat Technical University, Najaf, Iraq, in 2007, his master's degree in Communication Techniques Engineering from the University of Al-Furat Al-Awsat Technical, Engineering Technical College, Najaf, Iraq in 2020.He is currently work at Al-Furat Al-Awsat Technical University.

Hayder Jawad Albattat received a B.A.Sc. degree in Electrical Engineering Basra University, Iraq, M.Scs. in Electrical Engineering (Electronics and communication –Image Processing) Electrical engineering Department in Basra University, Iraq, and a Ph.D. degree in Electrical Engineering (Electronics and communication) – University of Basra, Iraq. He is currently an Asst. Professor in Electronic and Communication at Najaf Technical College / the Dpt. of Communication - Al-Furat Al-Awsat Technical University.

Hameed Rasool Farhan received his B.Sc., M.Sc. and Ph.D. degrees in electronic engineering from University of Technology, Baghdad, Iraq, in 1986, 2011, and 2018, respectively. He is currently a lecturer at the Electrical and Electronic Engineering Department, College of Engineering, University of Kerbala. His significant interests include Digital Electronics, DSP, Image Processing, Pattern Recognition, and Computer Vision.